tvst

Article

Depth-Dependent Corneal Biomechanical Properties in Normal and Keratoconic Subjects by Optical Coherence Elastography

Vinicius S. De Stefano[1,2], Matthew R. Ford[1], Ibrahim Seven[1], and William J. Dupps, Jr[1,3,4]

[1] Cole Eye Institute, Cleveland Clinic, Cleveland, OH, USA
[2] Department of Ophthalmology and Visual Sciences, Federal University of Sao Paulo, Sao Paulo, Brazil
[3] Department of Biomedical Engineering, Lerner Research Institute, Cleveland Clinic, Cleveland, OH, USA
[4] Department of Ophthalmology, Cleveland Clinic Lerner College of Medicine of Case Western Reserve University, Cleveland, OH, USA

Correspondence: William J. Dupps, Jr., Cole Eye Institute, Cleveland Clinic, 9500 Euclid Ave, i-32, Cleveland, OH 44195, USA. e-mail: bjdupps@outlook.com

Received: January 2, 2020
Accepted: April 7, 2020
Published: June 3, 2020

Keywords: corneal biomechanics; keratoconus; optical coherence tomography; elastography

Citation: De Stefano VS, Ford MR, Seven I, Dupps WJ Jr. Depth-dependent corneal biomechanical properties in normal and keratoconic subjects by optical coherence elastography. Trans Vis Sci Tech. 2020;9(7):4, https://doi.org/10.1167/tvst.9.7.4

Purpose: Compare depth-resolved biomechanical properties in normal and keratoconic corneas in live human subjects using optical coherence elastography (OCE).

Methods: In a prospective series of normal and keratoconus (KC) eyes, a corneal perturbation was applied by a custom swept-source OCE system using a transparent flat lens coupled to force transducers. Cross-correlation was applied to track frame-by-frame OCT speckle displacement. Regional displacements for the anterior and posterior stroma were plotted in force versus displacement (k) graphs. A spatial biomechanical property ratio (k_a/k_p) was defined by dividing the maximum total displacement by the maximum force for the anterior (k_a) and posterior cornea (k_p) and was compared between normal and KC groups with the Mann-Whitney U test. Area under the receiver operating characteristics curve (AUROC) for differentiating normal and KC eyes was calculated for k_a/k_p, k_{max}, and thinnest point of corneal thickness (TPCT).

Results: Thirty-six eyes were analyzed (21 eyes of 12 normal subjects and 15 KC eyes of 12 subjects). The k_a/k_p for the normal group was 1.135 ± 0.07 (mean $\pm$ standard deviation) and 1.02 ± 0.08 for the KC group ($P < 0.001$), indicating a relative deficit in anterior stromal stiffness in KC eyes. AUROC was 0.91 for k_a/k_p, 0.95 for k_{max}, and 1 for TPCT.

Conclusions: Significant differences in depth-dependent corneal biomechanical properties were observed between normal and KC subjects.

Translational Relevance: OCE was applied for the first time to human KC subjects and revealed alterations in the normal anterior-to-posterior stromal stiffness gradient, a novel and clinically accessible disease biomarker.

Introduction

Keratoconus (KC) is a major global cause of impaired vision and lost vision-related quality of life.[1–4] While an incidence of 1 in 2000 is frequently cited,[5] more recent analyses with modern tomographic diagnostics devices suggest that rates are much higher. Adult prevalence of KC was more recently measured to be 1 in 375 in a large European population,[6] and the prevalence of tomography-confirmed KC in Saudi children aged 6 to 21 years presenting to emergency departments for nonvisual complaints was an astounding 1 in 21 (nearly 12% in the 12–18 age group).[7]

Localized biomechanical abnormalities are believed to play a central role in the development of ectatic diseases such as KC and post-refractive surgery ectasia.[8–10] Cohesive tensile strength studies,[11] collagen microstructural evidence,[12,13] and finite element modeling sensitivity analyses[10,14] have previously suggested a role for regional weakening in the initiation of the topographic characteristics of corneal ectatic disease.

Despite broad acknowledgment that these diseases are disorders of mechanical disequilibrium, their diagnostic criteria are based primarily on static morphological features, such as curvature, elevation, and thickness, that do not incorporate biomechanical measurements.[5,15–19] Methods based on infrared reflectometry,[20] Scheimpflug imaging,[21,22] and optical coherence tomography (OCT)[23,24] have been developed to monitor corneal deformation behavior over very short time scales during an air puff perturbation, but only surface deformation is ascertained with these techniques. The development of clinical tools for spatially sensitive characterization of internal corneal deformation behavior represents an area of opportunity for enhancing the performance of screening paradigms and understanding the biomechanical underpinnings of progressive corneal warpage and thinning.

Methods have been introduced for measuring depth-resolved corneal mechanical properties nondestructively, but most reports are relegated to the ex vivo domain. Scarcelli and Yun published the first in vivo measurement of depth-dependent corneal biomechanical properties in a single human eye using Brillouin microscopy and observed a depth-dependent decline in Brillouin shift within a normal cornea.[25] In subsequent work, the group showed a higher rate of decline in depth-dependent Brillouin shift and significant spatial heterogeneity in ex vivo KC corneas obtained from deep anterior lamellar keratoplasty cases than in normal explants. In an 11-subject in vivo study, Brillouin shifts were lower in KC in the area of the cone but (1) were not reported as a function of depth for KC eyes and (2) demonstrated lower predictive value for disease discrimination than the standard tomographic indicators (maximum corneal curvature [k_{max}] and corneal thickness at the thinnest point).[26] A subsequent larger study similarly reported lateral (x and y, but not depth-dependent) differences in Brillouin spectroscopy values in normal and multistage KC subjects, and variables defined as differences in regional Brillouin properties between the corneal center and the periphery showed promise as a discriminative variable for KC.[27] This work supports the need for further examination of locally quantifiable biomechanical properties and their spatial relationships in KC.

Optical coherence elastography (OCE)[28] is an extension of the principle of ultrasound elastography[29] to OCT, wherein a series of images are acquired while inducing a mechanical perturbation.[11] Correlation analysis of speckle motion between frames enables micrometer-scale displacement sensitivity in various tissues, including the cornea.[30–33] We recently reported an OCE-based analysis of depth-dependent properties in a series of normal human subjects.[34] In the current study, we aim to prospectively characterize the depth-dependent axial deformation behavior in live human subjects with and without KC and compare anterior-to-posterior property distributions between groups.

Methods

A total of 24 patients (21 eyes from 12 normal subjects and 15 eyes from 12 subjects diagnosed with KC) were recruited over the course of 18 months in this prospective clinical study. Normal subjects were identified as those who were deemed suitable for laser in situ keratomileusis (LASIK) in a dedicated refractive surgery screening clinic at the Cleveland Clinic Cole Eye Institute. All subjects were assessed by a subspecialty-trained cornea and refractive surgeon (WJD), and the diagnosis of keratoconus was based primarily on tomographic evidence of anterior corneal steepening and supported by the presence of other signs of KC, such as colocalized corneal thinning and posterior elevation. Equivocal or suspect cases of KC were not specifically sought for this study, though a range of manifest tomographic presentations are represented (Table). An ophthalmologic examination was performed that included intraocular pressure (IOP) measurement obtained with the Food and Drug Administration–approved version of the Corvis (Oculus, Wetzlar, Germany) and corneal tomography using the Pentacam HR (version 1.21r43, Oculus). Both eyes of all recruited patients were measured, except eyes that had exclusionary findings, including history of ocular trauma, scar, or previous eye surgery. The study was approved by the Cleveland Clinic Institutional Review Board (IRB #13-213) and all participants provided informed consent for research. All the procedures were conducted according to the Declaration of Helsinki. The study was registered at clinicaltrials.gov (NCT03030755).

As described in a previous study,[34] the OCE system consisted of a custom-built swept source (HSL-20, Santec, Kamaki, Japan) OCT system with a center wavelength of 1310 nm, 15 mW of optical power, a 9-µm axial coherence length in air, a spot size of approximately 20 µm in air, and a scanning range of 15 x 15 mm laterally. The OCT imaging was performed using a previously described technique,[30] which consists of a fixed size scanning window (5-mm width) with lateral oversampling (~5x) to ensure accurate capture of the speckle pattern. Imaging was performed at a line rate of 100 k A-scans/sec

Table. Demographic, Tomographic, and Biomechanical Variables for Normal and Keratoconic Eyes

Patient	Sex	Eye	Age	Spherical Equivalent Manifest Refraction (D)	IOP (mmHg)	Scheimpflug Tomography			Elastography ka/kp
						Km (D)	k_{max} (D)	TPCT (μm)	
	Normal Subjects								
1	Male	OD	29	−4.38	15.5	41.6	42.5	529	1.156
		OS		−2.63	14.5	42.0	42.7	532	1.209
2	Male	OD	30	+0.75	17.0	39.3	39.7	590	1.118
		OS		+0.50	16.0	39.4	39.9	603	1.263
3	Female	OD	60	+3.00	15.5	42.2	43.0	543	1.146
		OS		+4.13	14.0	42.0	42.4	530	1.146
4	Female	OD	34	−0.50	13.0	41.9	43.3	529	1.196
		OS		−0.75	13.0	42.2	43.7	526	1.130
5	Female	OD	32	−4.13	17.0	41.8	43.0	535	1.008
		OS		−3.38	16.0	42.2	43.3	538	1.065
6	Male	OS	26	−1.00	19.0	42.0	43.0	559	1.048
7	Female	OS	32	−2.88	14.5	42.5	43.2	509	1.132
8	Female	OD	31	−6.00	15.0	46.6	47.1	542	1.089
		OS		−6.25	15.0	46.7	47.2	537	1.094
9	Male	OS	23	−0.25	18.5	44.7	45.4	591	1.093
10	Male	OD	39	−3.63	12.5	45.3	46.0	536	1.095
		OS		−3.63	11.5	45.5	46.4	535	1.108
11	Male	OD	35	+1.75	17.5	42.2	42.8	558	1.218
		OS		+2.13	16.0	42.1	43.1	543	1.313
12	Female	OD	34	−6.75	18.5	42.4	42.9	586	1.122
		OS		−7.13	19.0	42.8	43.5	596	1.090
	Keratoconus Subjects								
13	Male	OD	42	−2.38	16.8	48.7	66.30	390	1.055
14	Male	OS	55	−12.50	15.4	47.7	56.00	479	1.013
15	Female	OD	39	+0.25	17.6	43.8	48.20	497	1.000
16	Female	OD	59	0	14.0	44.3	44.70	506	1.049
		OS		−0.25	17.0	45.0	45.18	489	1.071
17	Female	OD	43	−0.63	7.0	46.2	54.70	442	1.151
18	Female	OS	34	0	10.0	52.2	58.30	448	1.063
18	Male	OD	42	−0.38	11.0	48.0	54.60	464	1.063
19	Male	OD	27	+2.75	11.2	52.6	63.0	398	1.044
		OS		+1.25	11.6	46.1	56.10	423	0.977
20	Female	OS	23	+1.88	9.0	51.8	69.50	464	0.889
21	Male	OD	21	−0.63	16	43.5	51.20	495	1.051
		OS		−1.00	17.5	43.3	50.50	482	1.045
22	Male	OD	57	+1.75	11	47.5	59.90	413	0.800
23	Male	OD	28	−2.75	10	43.4	43.90	473	1.041
	Controls (mean ± SD)		34 ± 9	−1.95 ± 3.29	15.6 ± 2.2	42.7 ± 2.0	43.5 ± 2.0	550 ± 27	1.14 ± 0.07
	Keratoconus (mean ± SD)		39 ± 15	−1.10 ± 3.54	13.0 ± 3.5	46.9 ± 3.3	54.8 ± 7.8	458 ± 37	1.02 ± 0.08
	P value[b]		0.26	0.07	0.015[a]	< 0.01[a]	< 0.01[a]	< 0.01[a]	< 0.01[a]

Subjects 1–12, normal group; 13–22, keratoconus group.
Km, mean keratometry.
[a]Statistically significant difference.
[b]Mann-Whitney *U* test.

across the 5-mm scan region with 2-μm lateral sampling and no averaging. Patients were given a drop of topical anesthetic (proparacaine hydrochloride 0.5%), then supported using a bite plate with a disposable single-use cover to stabilize the skull and minimize head motion. A visual fixation target was used to facilitate repeatable alignment with the OCT sample arm. A precision linear displacement stage (ViX 200m, Parker Hannifin, Cleveland, OH) controlled the corneal perturbation interface—a flat lens, 3 mm in thickness and tilted slightly relative to the sample arm to minimize reflection artifact—which was axially displaced in a continuous fashion through a total range of 2 mm over approximately 2 seconds. One hundred image frames (B scans) were acquired across the horizontal meridian, and highly sensitive force sensors (LSB200, Futek, Irvine, CA) provided real-time measurement of the force generated by the contact

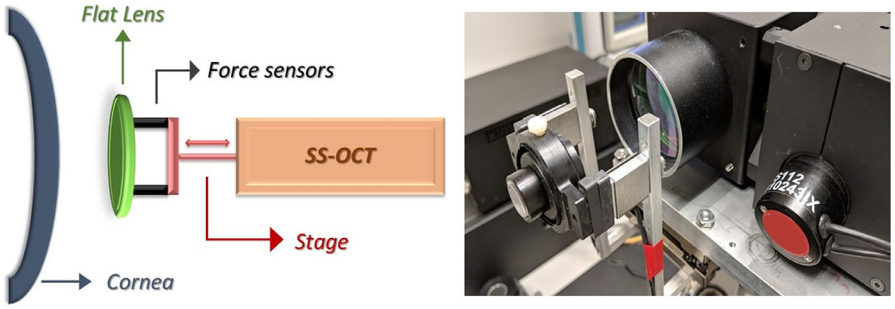

Figure 1. *Left*: schematic representation of the optical coherence elastography system. *Right*: picture of the prototype, with a focus on the transparent flat lens, force sensors, and translational stage. SS-OCT, swept-source optical coherence tomography system.

of the flat lens with the cornea. The flat lens was cleaned before every use with 70% isopropyl alcohol wipes.[35] Figure 1 provides a schematic overview and photograph of the clinical system.

Displacement tracking based on the OCT speckle pattern was performed in a frame-by-frame fashion on the raw OCT images as described in detail previously.[30] Custom software applied a normalized cross correlation algorithm to track the 2-dimensional (axial and lateral) motion of speckle on an interframe basis across all two-dimensional (2D) OCT images in the measurement sequence. This analysis was applied to temporally adjacent images using a 22 x 22 pixel window from the first image that was scanned systematically around the same spatial origin in the second image. The cross-correlation algorithm was used to determine the maximum likelihood displacement vector for the speckle pattern between the two images. This was repeated for the entire measurement sequence to generate pointwise cumulative (total) displacement data. Resulting displacement data for any given spatial location were rejected if the correlation coefficient did not reach a previously established quality value of ≥ 0.6.[30]

After displacement tracking, the time-synced data from the force sensors were plotted against the cumulative displacement data to generate an analogue of axial stiffness, $k = f/d$, where f is the force resulting from progressive contact between the flat lens and the anterior cornea and d is the local cumulative displacement of the cornea derived from OCT speckle tracking. Since the force/displacement relationship evolves temporally across the compression sequence, k was defined as the slope of a linear fit to the force and displacement data for the entire sequence.[34] Color maps displaying local displacement and k values across the cornea along with a depth-dependent k profile were generated for each eye in both groups. For color map generation, window sizes were set to 80 µm axially x 120 µm laterally to maximize visualization of local properties while maintaining adequate noise suppression. Two regions 1.6 mm wide x 150 µm deep (axial depth) representing the anterior and posterior thirds of the stroma were also defined, and k values were averaged across each region to produce an anterior (k_a) and a posterior (k_p) axial stiffness metric. The regions were separated axially by approximately 120 µm. The ratio of average axial stiffness for the two stromal regions, k_a/k_p, was then calculated and used for statistical comparisons of the property distributions of normal and KC groups. A k_a/k_p ratio of 1 indicates equivalent axial stiffness properties in both regions, whereas values greater than 1 indicate a stiffer anterior stroma and values less than 1 indicate a stiffer posterior stroma.

To assess the repeatability of the k_a/k_p measure within this study sample, three replicate measurements were obtained for each eye by the same observer, and the within-subject standard deviation (S_w) and intraclass correlation coefficient (ICC) were calculated across both groups.[36] A Mann-Whitney U test was performed to compare k_a/k_p values between normal and keratoconic corneas. A receiver operating characteristic (ROC) curve was constructed based on the KC and normal eye groups, utilizing a simple threshold of the k value as the discriminating variable. Statistical analyses were performed with SPSS Statistics 20 (IBM, Armonk, NY) and Minitab 19 (Minitab, State College, PA).

Results

Descriptive clinical and tomographic data for all eyes along with a statistical comparison of each parameter are detailed in the Table. Three replicate measures of k_a/k_p were obtained for each eye and yielded

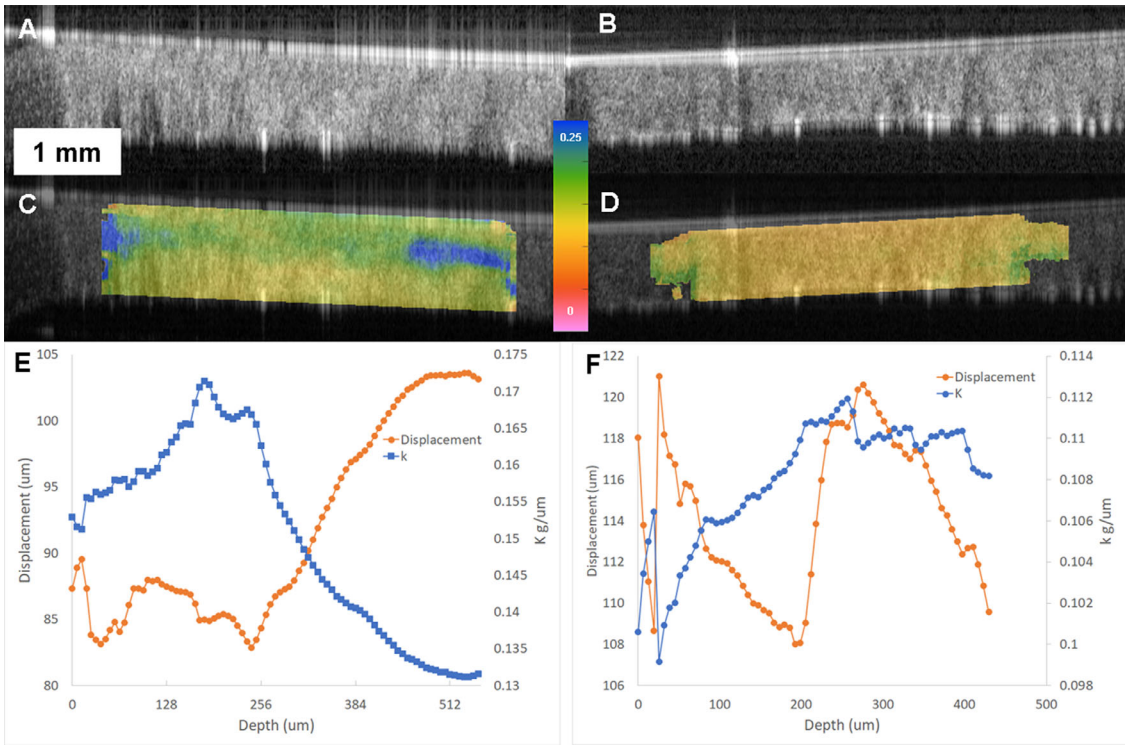

Figure 2. Examples of OCT elastography results for a normal eye (*left column*, panels A, C, E) and a keratoconus eye (*right column*, panels B, D, F). *A, B*: Corneal OCT scan obtained at the end of the elastography displacement series, capturing a full-thickness horizontal cross-section spanning a 5-mm width. Speckle tracking of raw OCT data was performed as described in the methods to derive displacement vectors. *C, D*: Map of OCT elastography–derived *k* values (local force/axial displacement relationship in grams/micrometer) overlaid on the raw OCT image. Color maps are on the same scale and demonstrate much lower (*red*) axial stiffness properties (*k*, in grams/micrometer) in the keratoconic eye than in the normal eye as well as absence of the relative anterior stromal stiffness advantage in keratoconus. *E, F*: Plot of depth-resolved displacement (*red*) and *k* (*blue*) values through a central corneal region of interest for the same eyes as in A–D. The scales in E and F differ and are normalized for each eye to highlight depth-dependent property differences. The magnitudes indicate higher axial displacements (*left axis*) at all depths in the keratoconic cornea and much lower force-to-displacement relationships (axial stiffness) through the keratoconic cornea (*right axis*). In addition to the differences in magnitudes, note the inversion of the normal anterior-to-posterior stromal stiffness distribution in keratoconus (*blue tracing* trending upward rather than downward toward the posterior stroma). This phenomenon drives significant group differences in the anterior-posterior ratio of *k* values (k_a/k_p, described in the text).

S_w 0.021 and ICC 0.907 (95% confidence interval, 0.768–0.963). Examples of elastographic maps for a normal and a KC eye are shown in Figure 2. Raw OCT images are optimized for high speckle contrast rather than being filtered to remove speckle. Edge artifacts due to high optical power, a flat optical lens, and some uncompensated dispersion can be seen in the raw images but do not impact internal corneal displacement tracking. In the normal eyes, all eyes demonstrated a pattern of smaller displacements (higher *k*, cooler colors) in the anterior part of the corneal stroma and larger displacements in the posterior stroma. That pattern translates into bell-shaped profiles in the depth-resolved *k* graphs associated with each image, in which higher *k* values dominate until approximately 150 to 200 µm in depth, where the *k* value decreases. In the KC group, there is greater spatial heterogeneity in *k* and a loss of the normal pattern in the color maps and *k* profile graphs, which show peak *k* values much deeper in the stroma. Additional examples of normal and KC eyes are described in Figure 3.

A quantitative comparison of anterior-to-posterior *k* ratios between control and KC corneas was performed using the nonparametric Mann-Whitney *U* test. The mean k_a/k_p values were higher in the normal eyes (n = 21, mean ± standard deviation, 1.135 ± 0.07) than in the keratoconus eyes (n = 15, 1.02 ± 0.08), with $P < 0.001$. In ROC analyses to assess the discriminative performance of k_a/k_p against two common tomographic variables, the area under the ROC curve (AUROC) was 0.91 for k_a/k_p, 0.95 for k_{max}, and 1.0 for the thinnest point of corneal thickness (TPCT). There was no correlation between k_a/k_p and TPCT within the groups ($r = 0.05$, $P = 0.8$ for controls; $r = –0.03$, $P = 0.5$ for KC), and since TPCT values spanned over 100 µm in each group, it is unlikely that thickness alone

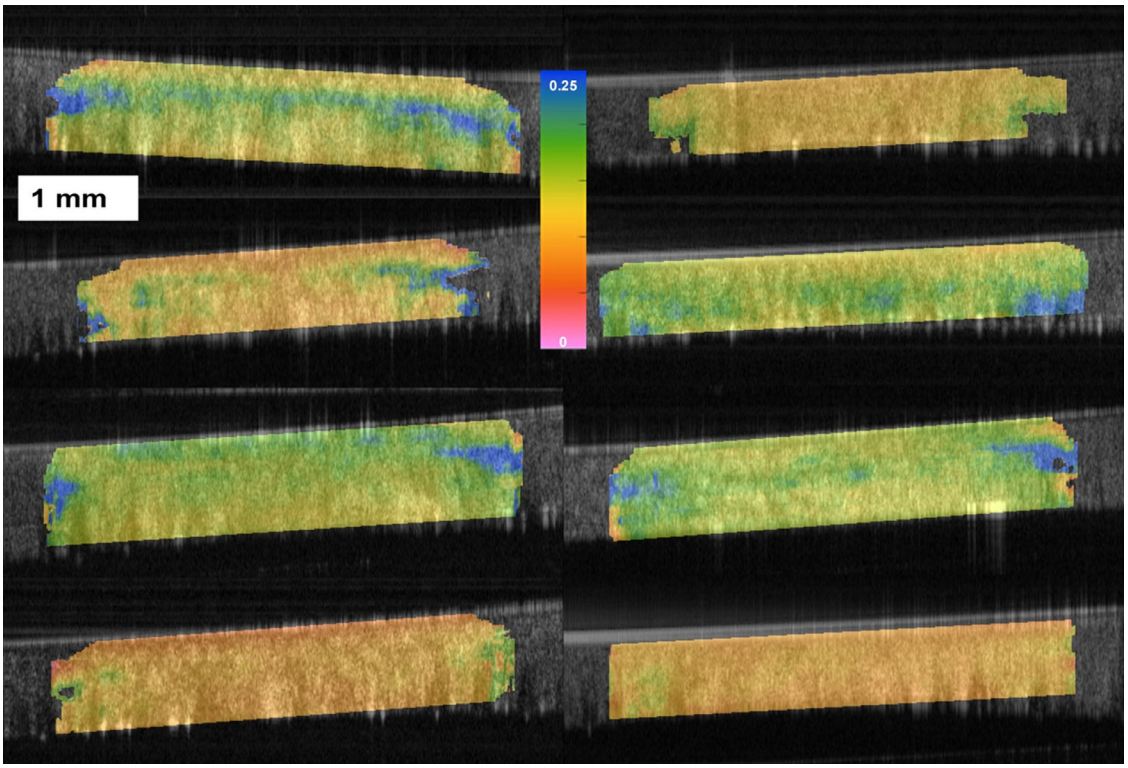

Figure 3. Additional elastograms of normal (*left column*) and keratoconus corneas (*right column*). The maps display *k* values (slope of the cumulative force/axial displacement relationship for each corneal point during the applanating perturbation) in grams/micrometer, and all share the same scale. Although a range of *k* value magnitudes are observed in both groups, normal corneas more consistently demonstrate a discrete band of higher (stiffer) *k* values (cooler colors) in the anterior one-third of the stroma, indicating less displacement and greater axial displacement resistance in that region. This preferential anterior stiffness is either absent or inverted in most keratoconus eyes, which tend to show a reduction in relative anterior stromal resistance to deformation.

can account for the anterior-to-posterior axial stiffness differences observed in this study.

Discussion

We present a comparative in vivo study using OCE to assess depth-dependent biomechanical differences between normal and keratoconic corneas. The observed differences not only have important clinical implications for potential enhancement of disease screening and selection of refractive surgery candidates, but they also present the first in vivo biomechanical evidence for a significant alteration in the normal depth-dependent distribution of corneal stromal properties in KC. Previous studies in human corneas, including work summarized earlier and other evidence from ultrastructural hydration studies[37] and acoustic radiation force elasticity imaging, have indirectly or directly suggested an elasticity gradient within the cornea, with higher relative strength in the anterior stroma than the posterior stroma. However, such work was performed primarily in nonkeratoconic ex vivo human corneal tissue, and no prior study has addressed the depth-dependent properties in living eyes of KC subjects.

An important distinction and advantage of in vivo measurement is the preservation of the in situ corneal anatomic boundary conditions and hydration, both of which are significantly altered by corneal removal and storage. All mechanical characterization techniques are sensitive to corneal hydration status, and this has been shown to be true in human corneas using OCE[38] and Brillouin scattering.[39] Donor globe studies[40] and computational models[41,42] have also demonstrated important dependencies between corneal biomechanical behavior and the presence and properties of the corneal limbus and sclera, so data obtained from excised corneas that are exposed to various experimental protocols affecting hydration could lead to different estimates of the cornea's biomechanical behavior. The relatively high level of repeatability of the k_a/k_p metric suggests that the 2-second perturbation/measurement

sequence does not result in significant dehydration artifact even with triplicate measurements.

Although the current methodology is notably different from noncontact Brillouin optical scattering, we observed similar trends in anterior-to-posterior stiffness behavior in normal eyes. Of the sparse available literature on depth-dependent human corneal properties, the most mechanically analogous testing regime to the OCE method used in this study and our precedent study in normal eyes[34] is an indentational perturbation that was applied axially (perpendicular to the collagen lamellar orientation) by Winkler et al. to femtosecond laser-dissected anterior, middle, and posterior stromal specimens of normal donor corneas.[43] The study demonstrated decreases in depth-dependent strength that mirrored those described by Randleman et al. using cohesive tensile testing[44]—a measure of peeling resistance rather than compressive axial resistance—and also correlated the axial compressive modulus to the density of collagen interweaving as measured by two-photon harmonic imaging. We suspect that the applanation-like perturbation used in the current study, which was well tolerated by patients after a drop of topical anesthetic, invokes resistance that depends on these same gradations in corneal ultrastructure by compressing the cornea against the intraocular pressure. The bending moments produced by the OCE perturbation are more complex than simple compression, however, and probably reflect a combination of compressive and shear resistance properties.

An important new finding in this study is the significant loss of this normal pattern of depth-dependence in live human KC corneas. While recent studies with Brillouin spectroscopy have confirmed the presence of spatially heterogeneous reductions in properties that localize *laterally* with the cone,[26,27,45] the current study provides a depth-dependent analysis and demonstrates a significant selective deficit in *anterior stromal* corneal properties. This finding could reflect the biomechanical consequences of structural decoupling of collagen lamellae in KC, a hallmark of which is the sparsity of transverse bridging fibers at the level of Bowman layer.[13] These transverse fiber populations are more abundant in the anterior stroma of normal corneas and correlate to axial stiffness properties,[43] so their absence in KC provides a potential source of compressive, cohesive, and shear weakness in the anterior stroma.[12,46] Histological descriptions of KC have also pointed to focal disruptions of Bowman layer and the epithelial basement membrane, and more recent studies suggest a variety of molecular interactions at the epithelial-stromal interface that may contribute to the pathogenesis of KC.[47–49] Late-stage reparative processes specifically targeting mechanical restoration of the anterior stroma, including localized fibrosis (apical scarring) or deposition of elastic microfibril bundles,[50] provide additional indirect evidence that focal anterior stromal weakening is a central disease feature in KC.

Another important implication of this work is that it provides a possible mechanism for posterior corneal surface elevation and localized thinning in KC that does not require loss of stromal collagen. Since OCE reveals an anterior deficit in axial compressive resistance in KC, it is likely that in the undeformed state, the outward force of the IOP against the posterior cornea would lead to unusually high compression of that region in KC eyes and secondary forward displacement of the posterior cornea (and thus thinning). This would be observable in clinical tomography as localized posterior surface elevation, a key morphological sign of KC.

If selective anterior stromal weakening is a feature of KC, there are additional implications for disease detection and refractive surgery screening. While air puff–based corneal deformation behavior can be useful for differentiation of clinically evident KC,[51,52] the ability to detect localized property abnormalities should support more sensitive, specific, and early detection of disease features. The current study was not designed to assess discriminative value in equivocal KC cases, but as the Table shows, our sample was not biased toward end-stage cases since most subjects were enrolled prior to planned treatment with corneal crosslinking rather than corneal transplantation. The AUROC value of 0.91 for k_a/k_p in this series was comparable to two major diagnostic variables that are used for KC diagnosis and staging.[53] This is an encouraging finding given that (1) k_a/k_p measures a dynamic property that is distinct from information provided by static shape variables and (2) these measurements were obtained from horizontal, vertically centered 2D cross-sections that were standardized across eyes for reproducibility rather than specifically targeting the cone apex and presumed point of maximum weakness. Further optimization of the scan protocol and extension of the approach to full 3D analysis, especially in combination with tomographic evaluation, could further improve performance and support detection of even earlier biomechanical signs of disease.

The possibility that anterior stromal strength is affected early in the process of KC initiation and progression also impacts assumptions about the relative biomechanical advantage of intrastromal refractive surgery such as small incision lenticule extraction (SMILE).[54] SMILE has been shown in theoretical, computational, and clinical studies to confer a relative biomechanical advantage over

LASIK by preserving anterior stromal fiber continuity in normal eyes.[55–57] In cases where anterior stromal strength is selectively compromised, however, the margin of that advantage would be lower, and in cases where anterior properties are actually weaker than posterior properties (k_a/k_p <1, as was the case for several KC eyes in this study), photorefractive keratectomy would likely confer even greater stability advantages over LASIK and SMILE by ablating weaker stromal tissue that is less capable of effective load bearing. Since current clinical methods of biomechanical measurement do not provide the spatial contrast necessary to detect localized changes like those described in this series, approaches such as OCE that do incorporate such capabilities are an important focus of translational efforts.

The OCE approach described here has limitations. The method involves corneal contact, though the amount of deformation is similar to that used in applanation tonometry and does not produce a measurable increase in IOP in directly cannulated donor globes.[38] We have presented relative regional stiffness values measured in the axial dimension during an applanating maneuver. Like applanation tonometry, the resistive force is strongly influenced by the IOP, which can be a confounder of attempts to characterize constitutive properties apart from the influence of preloading.[58,59] By expressing stiffness as a relative anterior-to-posterior corneal ratio, the force values are divided out of the ratio, thus normalizing for occasional artifacts in absolute force measurement (e.g., from patient motion). Furthermore, since the anterior and posterior corneal regions are subjected to the same applanating force and IOP during a given measurement, the differential displacement behavior of these regions is preserved and therefore unlikely to be severely confounded by IOP in group comparisons of k_a/k_p. This subject was taken up in greater detail with supporting experiments and computational simulations in a prior report.[34] A simplifying assumption that is implicit to OCE and to this study is that stress is homogeneous, manifested across and throughout the cornea. While the comparative analysis emphasized displacements in the central cornea to minimize any bias associated with this assumption, actual internal stresses cannot be measured.

Finally, we limited our analysis to the axial component of the 2D displacement vector in this study. While the patient stabilization system and motion boundary imposed by the applanating lens provided very stable axial motion control, lateral motion artifact from microsaccades made interpretation of lateral displacement data difficult. Our prior OCE work in donor eyes suggests that lateral displacement data would likely provide additional information about changes in the corneal biomechanical state.[38] Efforts are underway to develop a three-dimensional (3D) OCE system that supports more comprehensive regional sampling, which would provide full 3D displacement behavior analysis and enhance diagnostic sensitivity and specificity by extending the analysis beyond a 2D cross-section to include the cone apex.

In summary, we have presented the first in vivo evidence of a selective weakening of the anterior stroma in KC eyes and demonstrated that it is a clinically accessible biomarker of disease.

Acknowledgments

Supported by Grant R01 EY023381, Ohio Third Frontier Innovation Platform Award TECH 13-059, Research to Prevent Blindness Unrestricted Grant to the Department of Ophthalmology of the Cleveland Clinic Lerner College of Medicine of Case Western Reserve University (RPB1508DM), NIH/NEI P30 Core Grant (IP30EY025585), Sara J. Cheheyl Fund for Ocular Biomechanics Research, and Pender Family Research Fund at the Cole Eye Institute.

Disclosure: **V.S. De Stefano**, None; **M.R. Ford**, Cleveland Clinic (P); **I. Seven**, None; **W.J. Dupps**, Cleveland Clinic (P), Alcon (C), Zeiss (C), Glaukos (C)

References

1. Mahdaviazad H, Bamdad S, Roustaei N, et al. Vision-related quality of life in Iranian patients with keratoconus: National Eye Institute Vision Function Questionnaire–25. *Eye Contact Lens*. 2018;44(suppl 2):350–354.
2. Saunier V, Mercier AE, Gaboriau T, et al. Vision-related quality of life and dependency in French keratoconus patients: impact study. *J Cataract Refract Surg*. 2017;43:1582–1590.
3. Kymes SM, Walline JJ, Zadnik K, et al. Changes in the quality-of-life of people with keratoconus. *Am J Ophthalmol*. 2008;145:611–617.
4. Kymes SM, Walline JJ, Zadnik K, et al. Quality of life in keratoconus. *Am J Ophthalmol*. 2004;138:527–535.
5. Rabinowitz YS. Keratoconus. *Surv Ophthalmol*. 1998;42:297–319.
6. Godefrooij DA, de Wit GA, Uiterwaal CS, et al. Age-specific incidence and prevalence of kerato-

conus: a nationwide registration study. *Am J Ophthalmol*. 2017;175:169–172.
7. Torres Netto EA, Al-Otaibi WM, Hafezi NL, et al. Prevalence of keratoconus in paediatric patients in Riyadh, Saudi Arabia. *Br J Ophthalmol*. 2018;102:1436–1441.
8. Sinha Roy A, Dupps WJ, Jr. Effects of altered corneal stiffness on native and postoperative LASIK corneal biomechanical behavior: a whole-eye finite element analysis. *J Refract Surg*. 2009;25:875–887.
9. Roberts CJ, Dupps WJ, Jr. Biomechanics of corneal ectasia and biomechanical treatments. *J Cataract Refract Surg*. 2014;40:991–998.
10. Gefen A, Shalom R, Elad D, et al. Biomechanical analysis of the keratoconic cornea. *J Mech Behav Biomed Mater*. 2009;2:224–236.
11. Smolek MK. Interlamellar cohesive strength in the vertical meridian of human eye bank corneas. *Invest Ophthalmol Vis Sci*. 1993;34:2962–2969.
12. Meek KM, Tuft SJ, Huang Y, et al. Changes in collagen orientation and distribution in keratoconus corneas. *Invest Ophthalmol Vis Sci*. 2005;46:1948–1956.
13. Morishige N, Wahlert AJ, Kenney MC, et al. Second-harmonic imaging microscopy of normal human and keratoconus cornea. *Invest Ophthalmol Vis Sci*. 2007;48:1087–1094.
14. Roy AS, Dupps WJ, Jr. Patient-specific computational modeling of keratoconus progression and differential responses to collagen cross-linking. *Invest Ophthalmol Vis Sci*. 2011;52:9174–9187.
15. Gomes JA, Tan D, Rapuano CJ, et al. Global consensus on keratoconus and ectatic diseases. *Cornea*. 2015;34:359–369.
16. Randleman JB, Dupps WJ, Jr., Santhiago MR, et al. Screening for keratoconus and related ectatic corneal disorders. *Cornea*. 2015;34:e20–e22.
17. Shetty R, Rao H, Khamar P, et al. Keratoconus screening indices and their diagnostic ability to distinguish normal from ectatic corneas. *Am J Ophthalmol*. 2017;181:140–148.
18. Reinstein DZ, Archer TJ, Gobbe M. Corneal epithelial thickness profile in the diagnosis of keratoconus. *J Refract Surg*. 2009;25:604–610.
19. Ambrosio R, Jr., Alonso RS, Luz A, et al. Corneal-thickness spatial profile and corneal-volume distribution: tomographic indices to detect keratoconus. *J Cataract Refract Surg*. 2006;32:1851–1859.
20. Luce DA. Determining in vivo biomechanical properties of the cornea with an ocular response analyzer. *J Cataract Refract Surg*. 2005;31:156–162.
21. Ambrosio R, Jr., Nogueira LP, Caldas DL, et al. Evaluation of corneal shape and biomechanics before LASIK. *Int Ophthalmol Clin*. 2011;51:11–38.
22. Hon Y, Lam AK. Corneal deformation measurement using Scheimpflug noncontact tonometry. *Optom Vis Sci*. 2013;90:e1–e8.
23. Dorronsoro C, Pascual D, Perez-Merino P, et al. Dynamic OCT measurement of corneal deformation by an air puff in normal and cross-linked corneas. *Biomed Opt Express*. 2012;3:473–487.
24. Alonso-Caneiro D, Karnowski K, Kaluzny BJ, et al. Assessment of corneal dynamics with high-speed swept source optical coherence tomography combined with an air puff system. *Opt Express*. 2011;19:14188–14199.
25. Scarcelli G, Yun SH. In vivo Brillouin optical microscopy of the human eye. *Opt Express*. 2012;20:9197–9202.
26. Scarcelli G, Besner S, Pineda R, et al. In vivo biomechanical mapping of normal and keratoconus corneas. *JAMA Ophthalmol*. 2015;133:480–482.
27. Shao P, Eltony AM, Seiler TG, et al. Spatially-resolved Brillouin spectroscopy reveals biomechanical abnormalities in mild to advanced keratoconus in vivo. *Sci Rep*. 2019;9:7467.
28. Schmitt JM. OCT elastography: imaging microscopic deformation and strain of tissue. *Optics Express*. 1998;3:199–211.
29. Ophir J, Cespedes I, Ponnekanti H, et al. Elastography: a quantitative method for imaging the elasticity of biological tissues. *Ultrason Imaging*. 1991;13:111–134.
30. Ford MR, Dupps WJ, Jr., Rollins AM, et al. Method for optical coherence elastography of the cornea. *J Biomed Opt*. 2011;16:016005.
31. Zaitsev VY, Matveyev AL, Matveev LA, et al. Optical coherence elastography for strain dynamics measurements in laser correction of cornea shape. *J Biophotonics*. 2017;10:1450–1463.
32. Larin KV, Sampson DD. Optical coherence elastography—OCT at work in tissue biomechanics [invited]. *Biomed Opt Express*. 2017;8:1172–1202.
33. Kennedy BF, Wijesinghe P, Sampson DD. The emergence of optical elastography in biomedicine. *Nature Photonics*. 2017;11:215–221.
34. De Stefano VS, Ford MR, Seven I, et al. Live human assessment of depth-dependent corneal displacements with swept-source optical coherence elastography. *PLoS One*. 2018;13:e0209480.
35. Junk AK, Chen PP, Lin SC, et al. Disinfection of tonometers: a report by the American Academy of

Ophthalmology. *Ophthalmology*. 2017;124:1867–1875.
36. McAlinden C, Khadka J, Pesudovs K. Precision (repeatability and reproducibility) studies and sample-size calculation. *J Cataract Refract Surg*. 2015;41:2598–2604.
37. Muller LJ, Pels E, Vrensen GF. The specific architecture of the anterior stroma accounts for maintenance of corneal curvature. *Br J Ophthalmol*. 2001;85:437–443.
38. Ford MR, Sinha Roy A, Rollins AM, et al. Serial biomechanical comparison of edematous, normal, and collagen crosslinked human donor corneas using optical coherence elastography. *J Cataract Refract Surg*. 2014;40:1041–1047.
39. Shao P, Seiler TG, Eltony AM, et al. Effects of corneal hydration on Brillouin microscopy in vivo. *Invest Ophthalmol Vis Sci*. 2018;59:3020–3027.
40. Metzler KM, Mahmoud AM, Liu J, et al. Deformation response of paired donor corneas to an air puff: intact whole globe versus mounted corneoscleral rim. *J Cataract Refract Surg*. 2014;40:888–896.
41. Sinha Roy A, Rocha KM, Randleman JB, et al. Inverse computational analysis of in vivo corneal elastic modulus change after collagen crosslinking for keratoconus. *Exp Eye Res*. 2013;113:92–104.
42. Nguyen BA, Roberts CJ, Reilly MA. Biomechanical impact of the sclera on corneal deformation response to an air-puff: a finite-element study. *Front Bioeng Biotechnol*. 2018;6:210.
43. Winkler M, Chai D, Kriling S, et al. Nonlinear optical macroscopic assessment of 3-D corneal collagen organization and axial biomechanics. *Invest Ophthalmol Vis Sci*. 2011;52:8818–8827.
44. Randleman JB, Dawson DG, Grossniklaus HE, et al. Depth-dependent cohesive tensile strength in human donor corneas: implications for refractive surgery. *J Refract Surg*. 2008;24:S85–S89.
45. Scarcelli G, Besner S, Pineda R, et al. Biomechanical characterization of keratoconus corneas ex vivo with Brillouin microscopy. *Invest Ophthalmol Vis Sci*. 2014;55:4490–4495.
46. Akhtar S, Bron AJ, Salvi SM, et al. Ultrastructural analysis of collagen fibrils and proteoglycans in keratoconus. *Acta Ophthalmol*. 2008;86:764–772.
47. Shetty R, Vunnava KP, Dhamodaran K, et al. Characterization of corneal epithelial cells in keratoconus. *Transl Vis Sci Technol*. 2019;8:2.
48. Shetty R, Rajiv Kumar N, Pahuja N, et al. Outcomes of corneal cross-linking correlate with cone-specific lysyl oxidase expression in patients with keratoconus. *Cornea*. 2018;37:369–374.
49. Sharif R, Hjortdal J, Sejersen H, et al. Human in vitro model reveals the effects of collagen cross-linking on keratoconus pathogenesis. *Sci Rep*. 2017;7:12517.
50. White TL, Lewis PN, Young RD, et al. Elastic microfibril distribution in the cornea: differences between normal and keratoconic stroma. *Exp Eye Res*. 2017;159:40–48.
51. Hallahan KM, Sinha Roy A, Ambrosio R, Jr., et al. Discriminant value of custom ocular response analyzer waveform derivatives in keratoconus. *Ophthalmology*. 2014;121:459–468.
52. Roberts CJ, Mahmoud AM, Bons JP, et al. Introduction of two novel stiffness parameters and interpretation of air puff–induced biomechanical deformation parameters with a dynamic Scheimpflug analyzer. *J Refract Surg*. 2017;33:266–273.
53. Belin MW, Duncan JK. Keratoconus: the ABCD grading system. *Klin Monbl Augenheilkd*. 2016;233:701–707.
54. Dupps WJ, Jr. Intrastromal lenticule extraction for refractive correction: can it raise the tide for refractive surgery? *J Cataract Refract Surg*. 2018;44:1059–1061.
55. Reinstein DZ, Archer TJ, Randleman JB. Mathematical model to compare the relative tensile strength of the cornea after PRK, LASIK, and small incision lenticule extraction. *J Refract Surg*. 2013;29:454–460.
56. Sinha Roy A, Dupps WJ, Jr., Roberts CJ. Comparison of biomechanical effects of small-incision lenticule extraction and laser in situ keratomileusis: finite-element analysis. *J Cataract Refract Surg*. 2014;40:971–980.
57. Guo H, Hosseini-Moghaddam SM, Hodge W. Corneal biomechanical properties after SMILE versus FLEX, LASIK, LASEK, or PRK: a systematic review and meta-analysis. *BMC Ophthalmol*. 2019;19:167.
58. Roberts CJ. Importance of accurately assessing biomechanics of the cornea. *Curr Opin Ophthalmol*. 2016;27:285–291.
59. Liu J, Roberts CJ. Influence of corneal biomechanical properties on intraocular pressure measurement: quantitative analysis. *J Cataract Refract Surg*. 2005;31:146–155.